Mapping impedance microstructures in rocks with acoustic microscopy

MANIKA PRASAD, Stanford University, Stanford, California, U.S.

Various methods can characterize microstructural properties of reservoir rocks with the ultimate goal of relating microstructure to seismic properties. Scanning electron microscopy, transmission electron microscopy, and optical microscopy have traditionally been used for such studies. They have identified lithology, pore space, interconnectivity of pores, grain size, and cementation as the most important factors controlling seismic wave velocity and attenuation. However, these techniques provide *qualitative* descriptions only. The acoustic techniques presented here, scanning acoustic microscopy (SAM) and acoustic sounding (AS), can map and, more importantly, *quantify* microstructure as variations in acoustic impedance.

Ultrasonic stress waves are sensitive to local variations in elastic properties and are therefore particularly suited for characterizing microstructural properties of reservoir rocks. Reflections from impedance boundaries in grains and between interfaces in the sample are used to construct the microstructural image.

This paper will show that acoustic microscopy can be a powerful tool for studying internal structure and pore geometry of reservoir rocks.

Working principles. Acoustic microscopy's basic principle is almost identical to that of reflection seismology. Images of surface and subsurface microstructures are prepared on the basis of reflected acoustic waves—that is, on the impedance changes in the sample. Acoustic waves on a sample are mode converted, partly transmitted into the sample, and partly reflected. The reflection coefficient and with it the signal intensity received by the transducer are determined by the elastic constants of the material. Changes in acoustic impedance in the sample that influence wave reflection characteristics can be studied by mapping the reflected waves.

Because the working frequency of the acoustic waves can be varied, their penetration depth into the sam-

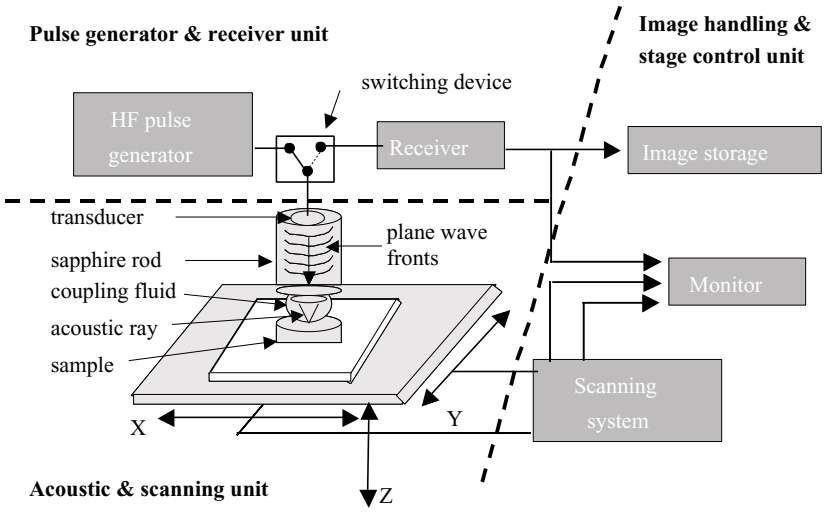

Figure 1. Diagram of an acoustic microscope. The Acoustic & Scanning Unit consists of a transducer, the acoustic lens, and a movable sample stage. The Pulse Generator & Receiver Unit emits short pulses to excite the transducer and receives and amplifies the reflected acoustic signals registered by the transducer. The Image Handling & Stage Control Unit controls stage motion and transforms the transducer signals to color scaled images with 512 pixels in x-y(z) directions with 8-bit resolution (256 colors). The transducer acts as a generator and receiver of acoustic waves. Acoustic waves reflected from sample surface and subsurface features carry impedance information. An acoustic image is made by registering the acoustic information as the acoustic lens carrying the transducer is scanned over the sample in x and y directions.

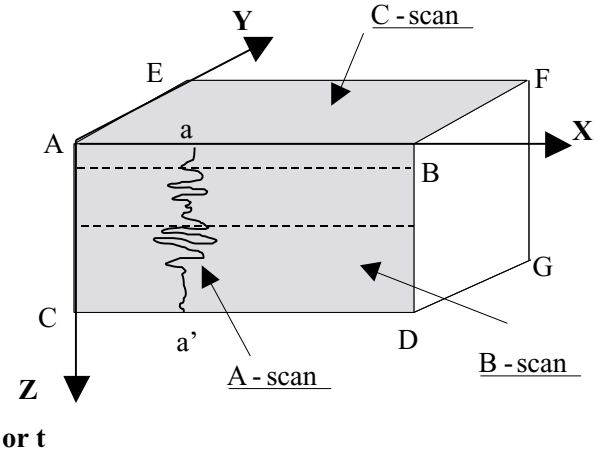

Figure 2. Types of scans obtained from acoustic imaging. An A-scan (a-a′) is an x-t scan similar to a seismic trace. B-scan "seismograms" (ABCD) are made with a moving (scanning) source and receiver. These scans are made by recording several A-scans through a time window with a fixed width along a line, similar to a seismic profile. In the figure, the dashed lines are schematic traces of layers, which can produce signals in the A-scan. A composite 3-D seismic image is created by combining profiles (B-scans) made at various locations (y positions). C-scans (ABEF) are x-y scans made at different, user-selectable time windows. These time windows correspond to depths (z positions) in the sample.

ple and the resolution of microstructural features can be controlled.

I will present results from high-frequency SAM (0.1-2 GHz) and low-frequency AS (25-100 MHz). The resolution of SAM is about 1 μm at 1 GHz; AS is some tens of micrometers (about 60 μm at 25 MHz). SAM and AS differ in the type of waves used. SAM images contain information from longitudinal and Rayleigh waves; AS images contain information from longitudinal waves only. The three main units (Figure 1) common to both systems are:

1) The Acoustic and Scanning Unit consists of a transducer to generate and receive acoustic waves, a sapphire rod as a wave guide, and a sample stage that can move in x, y, and z directions. Acoustic waves travel through the rod toward the sample. A cavity at the bottom of the sapphire rod focuses the waves through a coupling fluid (distilled water in this study) at a specific position on the sample. Reflected waves from the specimen return through the sapphire rod to the transducer, where they are converted into electrical signals. Together, the transducer, the sapphire rod, and the coupling fluid are referred to as the acoustic lens.
2) The Pulse Generator and Receiver Unit has a high-frequency pulse generator that emits short pulses to excite the transducer and a receiver that amplifies and records the signals received by the transducer. A switching device separates transmitted and received signals.
3) The Image Handling and Storage Control Unit is a computer-controlled scanning and image control system that allows stage manipulation and transforms electrical signals from the transducer into a gray- or color-scaled image. In this study, the image had 512 pixels in the x and y directions with 256 colors or gray shades. The lens is scanned in a raster pattern over the specimen in order to form an image.

The three main types of scans are (Figure 2):

- An A-scan or x-t scan (t = time). A one-dimensional A-scan is the primary information received at the transducer. It shows variations in signal amplitude with time received at a fixed lens position. Reflection seismic analog = a seismic line trace.
- A B-scan or an x-z scan. B-scans are made by recording several A-scans as the lens moves along a line. Any layering, alignment of grains and pores, clusters of grains with the same impedance can be mapped by these vertical 2-D scans. Reflection seismic analog = a seismic section.
- A C-scan or an x-y scan. C-scans gather information in a user-defined time window of the A-scan. The lens is moved in x and y directions. Data obtained at time t > 0 image a subsurface layer. Reflection seismic analog = side-scan sonar map.

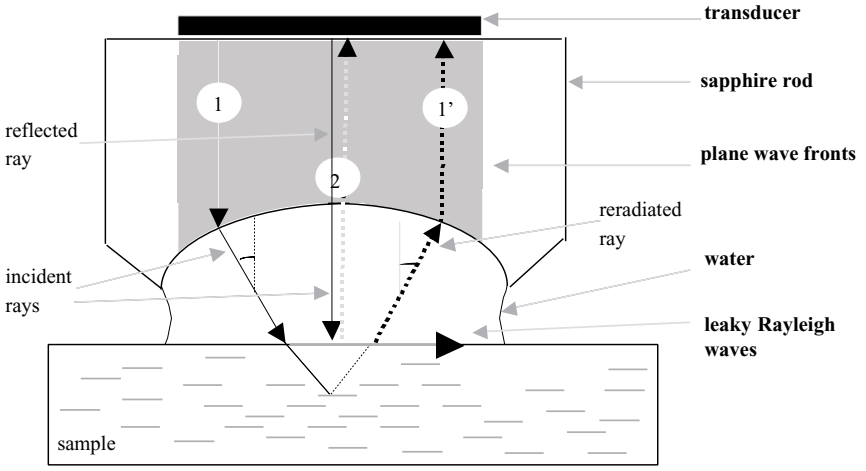

Figure 3. Diagram of raypaths. Acoustic waves generated by the transducer pass through the sapphire rod. The curvature at the end of the rod focuses the plane waves to a point on or below the sample surface. Stippled area shows the plane wave fronts, and dashed and solid lines trace the rays which carry information to the transducer. Ray 1 is incident at Rayleigh angle (θ_R) on the sample. These rays, incident at a Rayleigh angle of θ_R, generate Rayleigh waves which travel along path 1′ to the transducer. Ray 2 is a normally reflected ray. These two rays together contribute to the impedance information (adapted from Briggs, 1992).

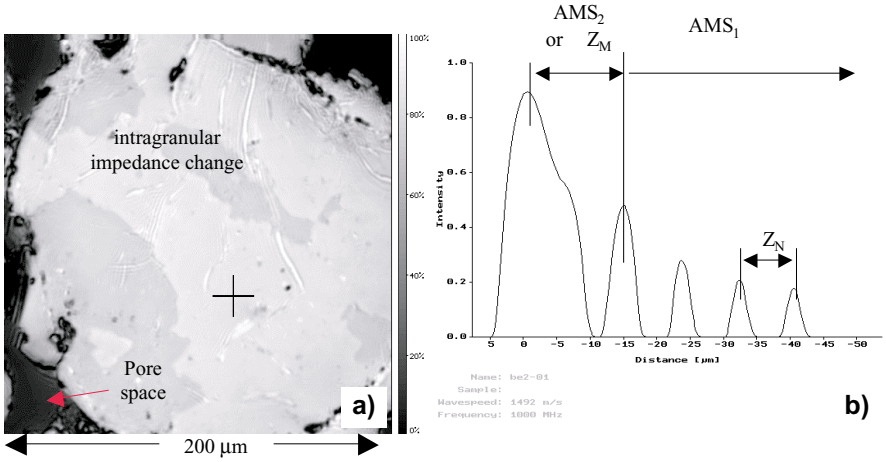

Figure 4. C-scan (a) and V(z) curve (b) in a Berea sandstone made at 1 GHz. The image of a quartz grain shows various gray shades due to different crystal axes alignments. A plus sign marks position of the V(z) curve in (b). Rayleigh wave velocity determined from the V(z) curve is 3.7 km/s.

Figure 3 shows a model of acoustic waves in SAM. The acoustic waves and raypaths are similar for AS (except that in latter, only longitudinal wave information is gathered). In the AS system, the microstructure is mapped by studying the reflections of longitudinal waves from the top and bottom of objects or layers with different acoustic impedance. In SAM, design and curvature of the high-frequency acoustic lens are optimized to also excite surface acoustic (Rayleigh)

waves in the surface of the sample. The SAM microstructural image is produced from the interference patterns between normally reflected longitudinal waves and the Rayleigh waves.

SAM. In acoustic imaging of materials with reasonable stiffness, such as rocks, a dominant role is played by Rayleigh waves which travel slower than longitudinal and shear waves and are confined within a depth of about a wavelength from the surface. Two raypaths (1-1′ and 2) are shown in Figure 3. The normally reflected longitudinal wave travels along path 2. The longitudinal wave traveling along path 1 is incident at a Rayleigh angle (θ_R) on the sample surface, where $\sin\theta_R = V_0/V_R$. V_0 = wave velocity in fluid and V_R = Rayleigh wave velocity in the sample. This ray excites Rayleigh waves in the surface of the sample which continuously leak energy back into the coupling fluid. These leaked waves travel back to the transducer as longitudinal waves along path 1′. The normally reflected longitudinal wave (path 2) and the longitudinal-Rayleigh-longitudinal wave (path 1-1′) contribute toward the signal received by the transducer and are summed with respect to amplitude and phase.

A surface image is produced when the acoustic beam is focused on the sample surface. A subsurface image is produced by moving the sample toward the lens such that the focal point of the acoustic beam is below the sample surface (Figure 3). Such a subsurface image is called a "defocused" image; "defocused" does not imply fuzzy.

A major cause of contrast in the acoustic images is the interference effect due to phase difference between the rays traveling along 1-1′ and 2. As the distance (z) between the lens and the sample is reduced, the longitudinal and Rayleigh waves change phase at different rates. Thus, with decreasing z, due to constructive and destructive interference between the two rays, the signal received by the transducer goes through a series of oscillations. This change in signal amplitude is called a V(z) curve. It denotes amplitude of signal received (V) as a function of distance (z) between lens and sample and is a material characteristic. The wavelength of the oscillation of this interference (Δz) is:

$$\Delta z = \frac{\lambda_0}{2(1-\cos\theta_R)}, \qquad (1)$$

Table 1. Velocity, density, acoustic impedance, and refraction index values of common rock-forming minerals. Color scale of the instrument is calibrated with materials of known impedance, and impedance variations in the sample are read from the color changes. Impedance values for calibration used here: 7-50.

Mineral	V_P km/s	V_S km/s	Density g/cm^3	Acoustic Impedance	Refractive Index
Quartz	6.04	4.09	2.65	16.0	1.55
Feldspars	5.59	3.06	2.56	14.3	1.52
	-7.05	-3.73	-2.73	-19.3	-1.57
Calcite	6.26	3.24	2.7	16.9	1.486
Dolomite	6.93	3.96	2.87	19.9	1.5
Pyrite	7.7	4.78	4.81	37.0	opaque
Clay	1.44	0.93	1.58	2.3	1.56
Carbon	4.26	2.68	1.47	6.3	opaque
Kerogen	2.25	1.45	1.3	2.9	opaque
Copper	4.759	2.325	8.933	42.5	

where λ_0 = *P*-wave length in coupling fluid, and θ_R = Rayleigh angle (Briggs. 1992).

From Snell's law ($\sin\theta_R = V_0/V_R$), V_R can be determined by:

$$V_R = V_0\left(1-\left(1-\frac{V_0}{2f\Delta z}\right)^2\right)^{-1/2}, \qquad (2)$$

where f = frequency and V_0 = wave velocity in fluid (from Briggs, 1992).

V_R can be calculated from the period of oscillations in the V(z) curve by equation 2. Figure 4a shows a C-scan image of a quartz grain, and Figure 4b its corresponding V(z) curve. The first large peak in the V(z) curve is registered at focus position; the crest is at z = 0. The crests and valleys mark constructive and destructive interference between longitudinal and Rayleigh waves at $z > 0$. V_R is calculated by determining the wavelength of this interference pattern (marked AMS_1) from Fourier analyses (Briggs, 1992).

V_R calculated from the V(z) curve marked AMS_1 in Figure 4b is 3.7 km/s, which is close to that of quartz (3.64 km/s).

V_R can also be determined from the V(z) curve at focus point. V_R is calculated from the distance between the maximum of specular reflection (at z=0) and the first interference maximum (Hirsekorn and Pangraz, 1994). This is AMS_2 in Figure 4b.

V_R calculated from AMS_2 part of the V(z) curve in Figure 4b is equal to 3.68 km/s.

The accuracy of V_R calculated with these methods is about 5%.

Interference patterns (called fringes) in C-scans can also yield V_R. At discontinuities, such as cracks or grain boundaries, interference between reflections from the surface and from the crack appear as fringes with a spacing (x),

$$x = \frac{\lambda_R}{2\sin\theta_c}, \qquad (3)$$

where λ_R = Rayleigh wavelength and θ_c = angle between crack and the sample surface. In case of vertical cracks ($\theta_c = 90°$), the relationship simplifies to $\lambda_R = 2x$ and

$$V_R = \lambda_R \cdot f = 2xf \qquad (4)$$

where f = frequency of measurement. Figure 5 shows an example of a cement mortar sample with Rayleigh fringes in a quartz grain. The prominent dark line in the middle of the image marks a discontinuity within the quartz grain. Rayleigh fringes are the less prominent lines running parallel to segments of the discontinuity. V_R determined from this method is 3.50 km/s. Due to uncertainties in measurement of the fringe spacing, this method has a large error in V_R. Due to digitization limitations and errors in locating the troughs (or peaks), errors in measuring x can be as large as 10%.

C-scans of surface and subsurface features can be used to study impedance changes in the sample. In essence, color changes in the acoustic images are used to study qualitative impedance changes. Once the gray-scale output of SAM is calibrated with materials of known impedance, impedance variations in unknown samples can be inferred from the calibrated gray scales.

Table 1 lists velocity, density, and impedance values of some rocks and common rock-forming minerals. Expected variations in the impedance

of reservoir rocks lie between 1.5 Mrayls (for water) and 35 Mrayls (for olivine). The gray scale of the SAM used here was calibrated using materials with impedance within this range (Figure 6). In this figure, the gray level from 0 (= black) to 255 (= white) is plotted as a function of reflection coefficient of the reference materials with respect to water. The least-squares linear fit (solid line) was used to evaluate impedance values in unknown samples. This method assumes minimal instrumental drift. However, approximately 10-15% error is to be expected, especially if calibrations are not performed at least daily or if the sample has large variations in surface topography.

Application to petrophysics. Rocks are composites in which the grains are cemented together by different clastic materials. The ultimate strength of the rock and its seismic properties strongly depend on the stiffness of grain-to-grain contacts. For example, Dvorkin and Nur (1996) have shown that velocity is dependent on the position of diagenetic cement: Higher velocity correlates with cement located at grain contacts, and lower velocity correlates with cement located away from the grain contacts. In a similar study, Avseth et al. (1998) used cathode-luminescent light to show that contact-cement rims around grains give higher *P*-wave velocity. Higher attenuation and lower velocity were measured in sandstones with large impedance difference between contact zone and grains (Prasad and Manghnani, 1997). A strong contact cement will lock in porosity and will resist porosity reduction under pressure. In the following, I compare seismic properties of two sandstones with their cementation strength inferred from acoustic microscopy.

Figure 7 shows typical 1 GHz C-scans of surface images in Berea and Boise sandstones. The gray scale is calibrated according to Figure 6. Pore spaces are dark gray to black; grains are gray. Feldspar grains have a pitted appearance due to alteration effects. Grain overgrowths are observed in both samples. However, in Berea sandstone, the contact zone is discontinuous and has significantly lower impedance change than the grains (Figure 7b). In Boise sandstone, the grains and the cement network that bridges across them have similar impedance (Figure 7d).

In Berea sandstone (Figures 7a and 7b), grains are rounded with smooth surfaces. Diffraction fringes are observed in the quartz grains as bright lines. Contacts between grains resemble cracks; they are flat and narrow. Color change (=impedance change) between grains and contact zone is high, indicating that the contacts are discontinuous and might close under pressure. In contrast, Boise sandstone (Figure 7c and 7d) has larger and angular grains with many overgrowths. The contact zone is broader with a cement network that bridges across the grains (Figure 7d). The intergranular bridges have similar impedance as the grains. There is significant microporosity in the cement.

The effect of contact impedance differences on seismic properties is demonstrated in Figure 8, where V_P and V_S are plotted as a function of pressure for both sandstones.

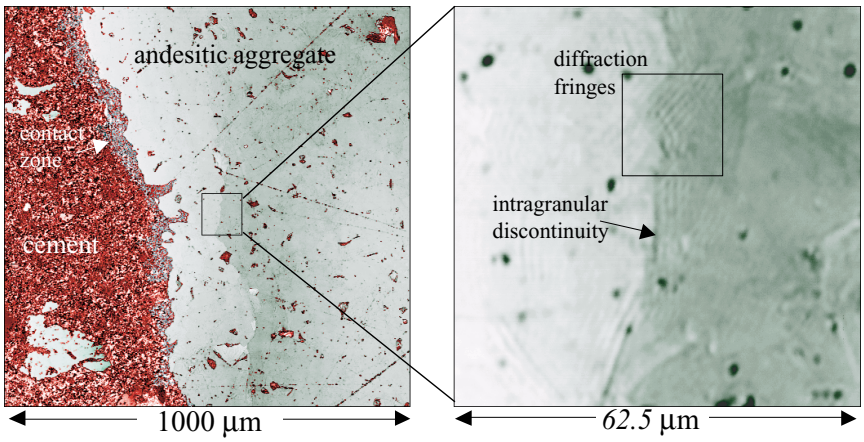

Figure 5. C-scan images of a mortar with andesitic aggregate and silica fume made at 1 GHz. The impedance is false-color-coded to enhance the impedance differences among the cement, contact zone, and the andesitic aggregates in the left image. The box in the center shows position of expanded view on the right. The intragranular discontinuity in the aggregate grain is seen as a color change. This discontinuity generates additional reflections which produce the typical interference fringe pattern observed here. The interference fringes are recognized at discontinuities as lines running parallel to the discontinuity (from Prasad et al., 2000).

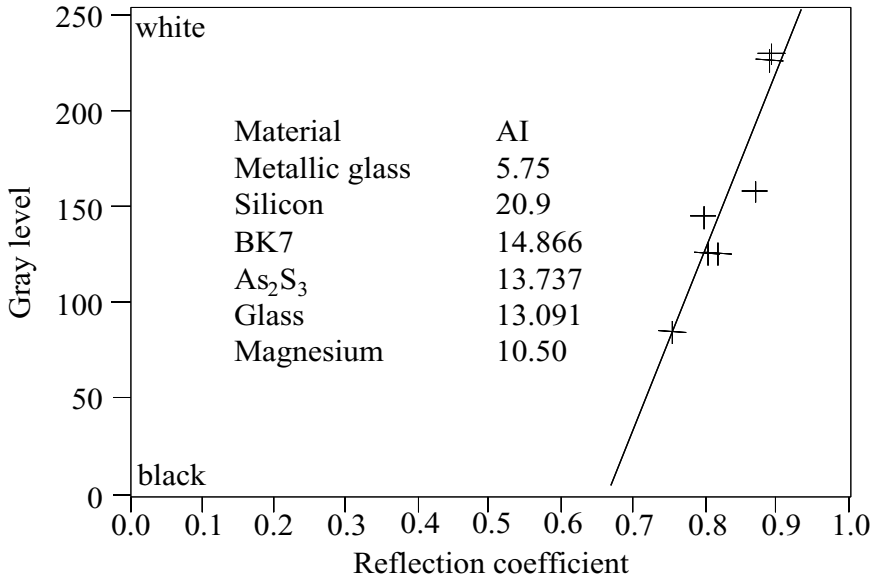

Figure 6. Gray-scale calibration of the high-frequency SAM instrument used for this study. The materials used for this calibration, along with their acoustic impedance values are listed in the adjoining table. The figure shows plot of reflection coefficients with respect to water against the gray level of the C-scan image made at one instrument setting.

Porosity, air permeability, V_P, V_S at 0 and at 40 MPa are given in Table 2. Velocity values are higher in the Boise than in the Berea sandstone. The high velocity at 0 MPa in Boise is related to the strong contact-cement network that increases frame rigidity. The same cement network resists deformation and so velocity does not change much with pressure. In Berea, due to more compliant contact cement, velocity change with pressure is pronounced. At higher pressures, it even surpasses velocity in Boise. This behavior is an experimental confirmation that contact-cement compliance defines the pressure dependence of bulk rock elastic properties.

Microstructural characteristics of organic rich shales can give important insights on the kerogen maturation processes. If microstructural variations can be related to bulk property measurements, indirect methods for detection of kerogen-rich shale sequences will be greatly enhanced. The opaque nature of the kerogen and the associated pyrite makes optical characterization rather difficult. Prasad and Nur (1997) have shown the importance of AM to study microstructure of kerogen-rich shales. They measured impedance of grains, grain clusters, and the matrix from AM images of shales with varying kerogen content and at different maturity grades. The impedance of the shale matrix was found to correlate with the total organic content and the hydrogen index of the shale.

Figures 9a and 9b show examples of SAM impedance and AS reflectivity results of a kerogen-rich shale. The very high reflectivity in the B-scans from AS are due to high-impedance contrast in the SAM images (Figure 9a) between grains (white) and matrix (black). Figure 9b represents an A-scan made at that position. Figures 9c and 9d are volumetric reconstructions from B-scans.

Figures 10a to 10c show acoustic sounding of a coal sample along with an optical line trace (10d) of its main features; the C-scan (Figure 10a) is a surface image and the B-scan (Figure 10b) is a zero-offset reflection profile. In analogy to reflection seismic mapping, reflections occur at interfaces with an impedance change. Continuous interfaces are mapped as layers in the B-scan. Layers can be mapped in three dimensions by combining multiple B-scans from different locations. Figure 10c is a reconstruction of a $30 \times 30 \times 8$ mm^3 volume of the sample created from 40 B-scan images. The dull and bright coal layers with different impedance imaged in the C-scans (Figure 10a) are seen to dip in the B-scans (Figure 10b) and in the reconstructed volume image (Figure 10c). Figure 10c also maps numerous cleats that cut across the dipping layers. The resemblance between the reconstructed top surface of the cube and the C-scan image of the same surface provides validity of the technique. "Ground truth" for the scans was seen from the line trace of the features made after cutting the sample to expose the sides (Figure 10d).

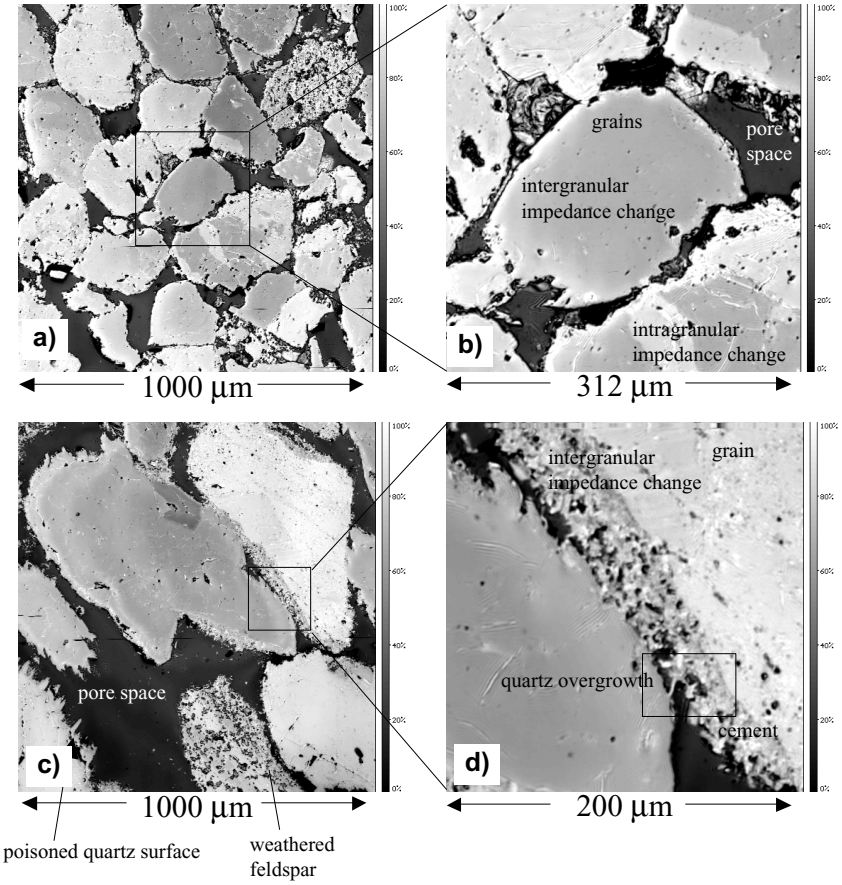

Figure 7. C-scans of Berea (a, b) and Boise (c, d) sandstones at different magnifications made at 1 GHz. Impedance is gray color-coded: white = high, black = low impedance according to the calibration in Figure 6. The images show various quartz and feldspar grains and the contact areas between them. The black areas are pore spaces; grains are gray. In Berea sandstone (a, b), the grains appear rounded; quartz grains do not show many overgrowths. Between adjacent grains, there is often a layer of cement with lower impedance (see detailed image in b). In Boise sandstone (c, d), quartz grains show typical "poisoned" surfaces, where overgrowths occur in fingers. The contact region between adjacent grains has numerous growths bridging the grains. The box in (d) shows an example of bridging cement between grains. Altered feldspar grains are recognized by strong intragranular impedance variations due to alteration and twinning effects.

Table 2. Velocity and quality factor measurements in Boise and Berea sandstone samples at 0 and 25 MPa confining pressure. Although at lower pressures Berea sandstone has lower velocity than Boise sandstone, the relation reverses under pressure (see also Figure 8).

	0 MPa		25 MPa		0MPa	
Sample	V_P	V_S	V_P	V_S	Porosity	Permeability
	(km/s)		(km/s)		(%)	(md)
Boise	3.849	2.083	4.085	2.229	25.8	902
Berea	3.305	2.010	4.164	2.565	22	381

Future work. The above examples show that acoustic microscopy has enormous potential for petrophysical studies. Using this technique, we can

- quantify microstructure in terms of elastic properties
- nondestructively map aligned grains, layers, and cracks to determine anisotropy
- map grain or pore clusters of comparable impedance that cause scattering losses
- measure cementation strength and predict seismic properties at depth
- measure Rayleigh wave velocity (used to estimate V_S) on a nanometer scale
- map and quantify inter- and intragranular defects
- measure elastic, anelastic, and adhesive surface properties of grain contacts

Because the same sample can be used for seismic measurements and for impedance analyses, the impedance microstructure can be related to reflection patterns, attenuation mechanisms, and bulk wave propagation characteristics. Such analyses are important in studying loss mechanisms and anisotropy and in characterizing wave propagation characteristics.

Despite their ubiquitous presence, studying clay minerals is a longstanding problem. Barring some estimates, single crystal elastic properties of clay minerals are almost nonexistent. Recent studies have shown that the dynamic Young's modulus can be measured on a nanometer scale (Rabe et al., 1996) with atomic force acoustic microscopy. Valuable future areas of study could include measurements of Young's modulus of clay minerals with atomic force acoustic microscopy, systematic analyses of seismic properties as a function of impedance changes related with different clay types and locations (as cement or as pore filling), changes in acoustic impedance, and effect of maturation on microstructure of kerogen-rich shales.

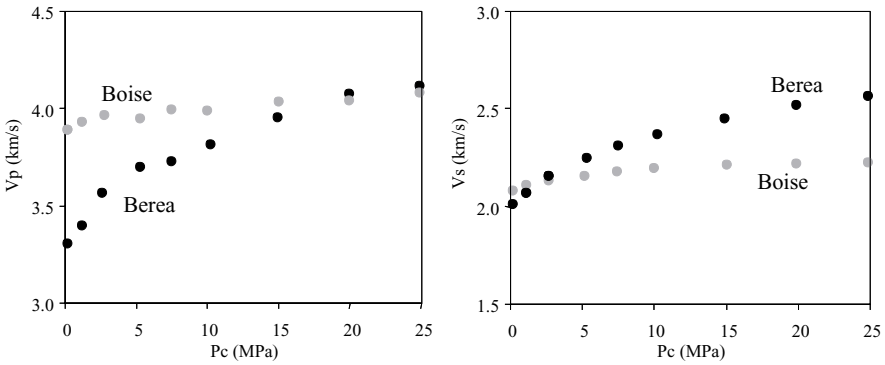

Figure 8. V_P and V_S as function of pressure in Berea and Boise sandstones. The measurements were made at room dry conditions. Velocity in Berea increases significantly with pressure; it does not change much in Boise.

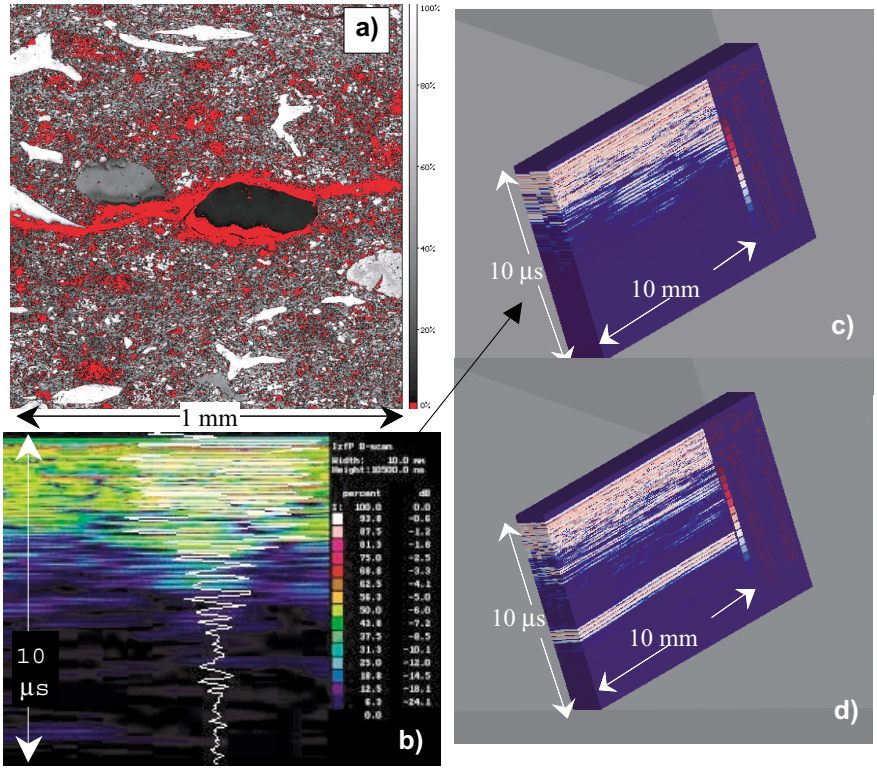

Figure 9. Comparison between SAM impedance microstructure made at 1 GHz (9a) and AS reflectivity (made at 15 MHz) (9b) of a kerogen-rich shale. 3-D reconstructions are shown in 9c and 9d. Lowest impedance (less than 7.5) is masked by red in Figure 9a. The 15 MHz AS images (c and d) are made of the same sample from opposite directions. Top image has coarse-grained, high-impedance layer from Figure 9a on top (contact is at 5.5 mm = 1.4 s). Bottom image has the coarse-grained, high-impedance layer at bottom (contact is at 22.7 mm = 6 s). A prominent reflection from this contact is seen only in the bottom image. Scattering from the coarse-grained layer in the top image masks it. The white line in the single B-scan at left is the line trace of a single A-scan.

Suggested reading. "Diagnosing high-porosity sands for reservoir characterization using sonic and seismic" by Avseth et al. (SEG 1998 *Expanded Abstracts*). *Acoustic Microscopy* by Briggs (Oxford, 1992). "Elasticity of high-porosity sandstones: theory for two North Sea data sets" by Dvorkin and Nur (GEOPHYSICS, 1996). "Materials characterization with the acoustic microscope" by Hirsekorn and Pangraz (*Applied Physics Letters*, 1994). "Applications of scanning acoustic microscopy to reservoir rocks" by Prasad (SEG 1997 *Expanded Abstracts*). "Velocity and impedance microstructural anisotropy in reservoir rocks" by Prasad and Manghnani (SEG 1996 *Expanded Abstracts*). "Effects of pore and differential pressures on compressional wave velocity and quality factor on Berea and Michigan sandstones" by Prasad and Manghnani (GEOPHYSICS 1997). "Scanning acoustic microscopy for evaluating interfacial bonds and

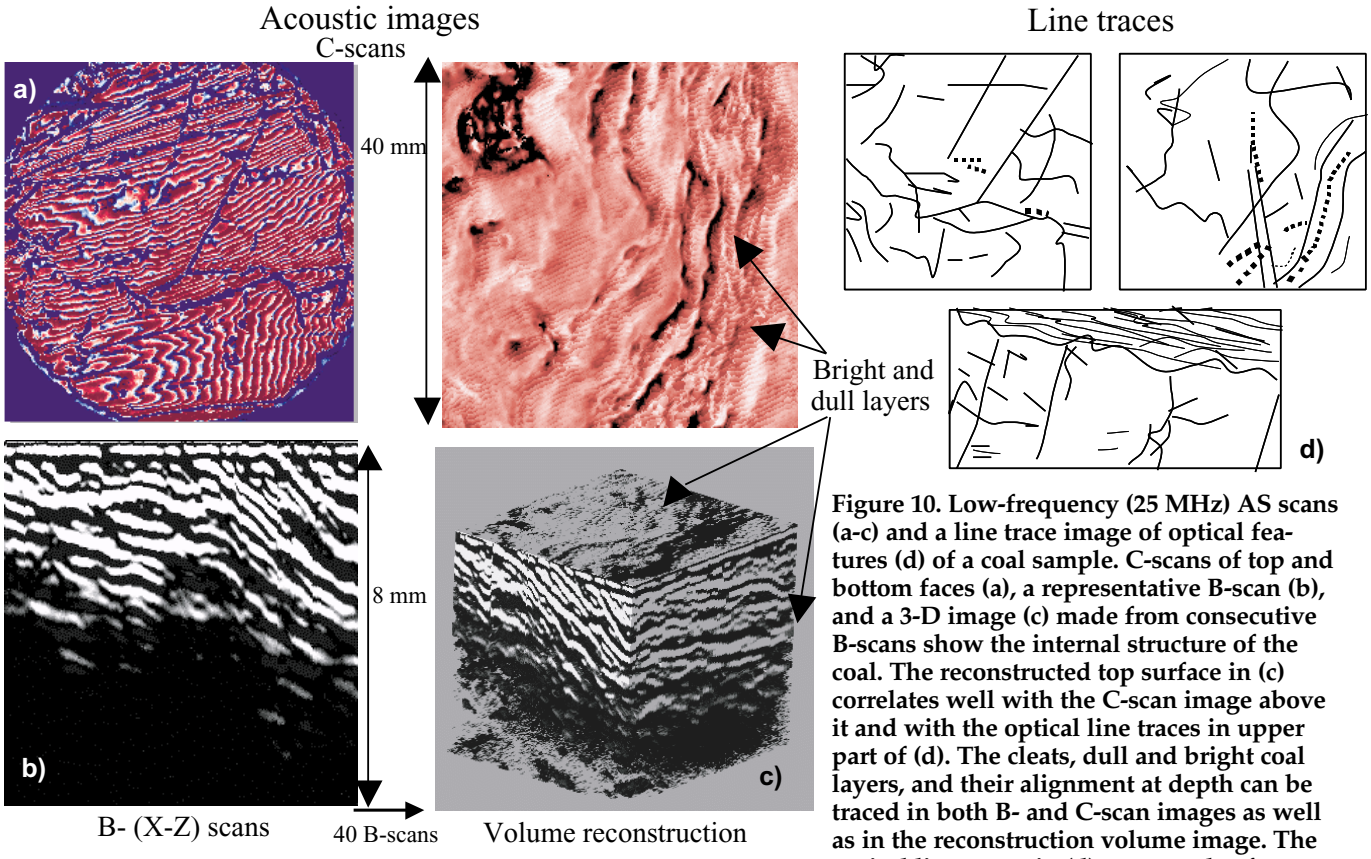

Figure 10. Low-frequency (25 MHz) AS scans (a-c) and a line trace image of optical features (d) of a coal sample. C-scans of top and bottom faces (a), a representative B-scan (b), and a 3-D image (c) made from consecutive B-scans show the internal structure of the coal. The reconstructed top surface in (c) correlates well with the C-scan image above it and with the optical line traces in upper part of (d). The cleats, dull and bright coal layers, and their alignment at depth can be traced in both B- and C-scan images as well as in the reconstruction volume image. The optical line traces in (d) were made after cutting the sides of the coal sample. They show ground truth for the scans and for the 3-D reconstruction.

microstructure in Portland cement concrete" by Prasad et al. (*Journal of Materials Science*, 2000). "Analyses of impedance microstructure of kerogen rich shales using scanning acoustic microscopy" by Prasad and Nur (*EOS*, 1997. "Acoustic microscopy with resolution in the nm-range" by Rabe et al. (*Acoustical Imaging*, 1996). "Acoustic microscopy of rocks" by Rodriguez-Ray et al. (*Journal of Microscopy*, 1990). E

Acknowledgments: This work is supported by the SRB Project, ARCO oil company, and NSF grant EAR-0074330. The coal scans were made at the University of Hawaii. The acoustic microscopy was done at the Fraunhofer Institute for Nondestructive Testmethods (IzfP) in Germany, and some at the University of Hawaii. I thank Walter Arnold (IzfP), Andrew Briggs, Silvia Fassbender, and Amos Nur for very helpful discussions and suggestions, Klaus Krämer for support in using the instruments. For the coal sample analyses, I thank Murli Manghnani and Amoco Oil Company for support during my stay at the University of Hawaii as a visiting scientist.

Corresponding author: M. Prasad, manika.prasad@stanford.edu